John von Neumann Institute for Computing

Ab Initio Molecular Dynamics and Ab Initio Path Integrals

Mark E. Tuckerman

published in

Quantum Simulations of Complex Many-Body Systems: From Theory to Algorithms, Lecture Notes,
J. Grotendorst, D. Marx, A. Muramatsu (Eds.),
John von Neumann Institute for Computing, Jülich,
NIC Series, Vol. **10**, ISBN 3-00-009057-6, pp. 299-324, 2002.

© 2002 by John von Neumann Institute for Computing
Permission to make digital or hard copies of portions of this work for personal or classroom use is granted provided that the copies are not made or distributed for profit or commercial advantage and that copies bear this notice and the full citation on the first page. To copy otherwise requires prior specific permission by the publisher mentioned above.

http://www.fz-juelich.de/nic-series/volume10

Ab Initio Molecular Dynamics and Ab Initio Path Integrals

Mark E. Tuckerman

Department of Chemistry and Courant Institute of Mathematics
New York University, New York, NY 10003, USA
E-mail: mark.tuckerman@nyu.edu

1 Introduction

Modern theoretical methodology, aided by the advent of high speed computing, has advanced to a level that the microscopic details of chemical events can now be treated on a routine basis. One of the most important development in this area has been the so called *ab initio* molecular dynamics (AIMD) method[1], which combines finite temperature atomistic molecular dynamics with internuclear forces obtained from accurate electronic structure calculations performed "on the fly" as the MD simulation proceeds. Finally, the combination of AIMD with the discrete path integral gives rise to a very powerful technique for studying chemical processes in which nuclear quantum effects play an important role.

AIMD has been used to study a wide variety of chemically interesting systems. These include, but are certainly not limited to, calculations of the structure and infrared spectroscopy of water[2,3], proton transport in aqueous acidic and basic environments[4–7], proton order/disorder and infrared spectroscopy of ice[8,9], structure of liquid silicates[10,11], structure and ionic solvation in liquid ammonia[12,13], calculation of NMR in proteins[14] and structure of nucleic acids[15], Ziegler-Natta catalysis[16], and proton transport in methanol and methanol/water mixtures[17], to name just a few examples. The wide variety of applications attests to the power and flexibility of the AIMD and *ab initio* path integral (AIPI) approaches.

For reasons of computational efficiency, the most commonly employed approach to AIMD is based on a density functional representation of the electronic structure and expansion of the electronic orbitals in a plane wave basis set, and this is the approach on which we shall focus in this lecture. However, it is important to note that AIMD is a general approach, and a number of examples exist in the literature which employ more accurate or more empirical electronic structure methods[18,19] as well as different basis sets[20–22].

This lecture is organized as follows. We shall begin with a brief review of the Born-Oppenheimer approximation and show how the AIMD method naturally emerges. We shall then describe the adiabatic dynamics approach of Car and Parrinello[1] and arrive at the Car-Parrinello equations of motion. We shall then show how to derive a path integral version of the Born-Oppenheimer approximation and describe the incorporation of the AIMD methodology into the path integral scheme. Finally, we shall show how the Car-Parrinello method can be employed to yield an efficient AIPI algorithm.

2 The Born-Oppenheimer Approximation and *Ab Initio* Molecular Dynamics

Consider a system of N nuclei described by coordinates, $\mathbf{R}_1, ..., \mathbf{R}_N \equiv \mathbf{R}$, and momenta, $\mathbf{P}_1, ..., \mathbf{P}_N \equiv \mathbf{P}$ and N_e electrons described by coordinates, $\mathbf{r}_1, ..., \mathbf{r}_{N_e} \equiv \mathbf{r}$, momenta, $\mathbf{p}_1, ..., \mathbf{p}_{N_e} \equiv \mathbf{p}$, and spin variables, $s_1, ..., s_{N_e} \equiv s$ with a Hamiltonian of the form

$$H = \sum_{I=1}^{N} \frac{\mathbf{P}_I^2}{2M_I} + \sum_{i=1}^{N_e} \frac{\mathbf{p}_i^2}{2m} + \sum_{i>j} \frac{e^2}{|\mathbf{r}_i - \mathbf{r}_j|} + \sum_{I>J} \frac{Z_I Z_J e^2}{|\mathbf{R}_I - \mathbf{R}_J|} - \sum_{i,I} \frac{Z_I e^2}{|\mathbf{R}_I - \mathbf{r}_i|}$$

$$\equiv T_{\rm N} + T_{\rm e} + V_{\rm ee}(\mathbf{r}) + V_{\rm NN}(\mathbf{R}) + V_{\rm eN}(\mathbf{r}, \mathbf{R}) \tag{1}$$

where m is the mass of the electron, and $Z_I e$ is the charge on the Ith nucleus. In the second line, $T_{\rm N}$, $T_{\rm e}$, $V_{\rm ee}$, $V_{\rm NN}$, and $V_{\rm eN}$ represent the nuclear and electron kinetic energy operators and electron-electron, electron-nuclear, and nuclear-nuclear interaction potential operators, respectively. We begin by looking for the eigenfunctions and eigenvalues of this Hamiltonian, given by:

$$\left[T_{\rm N} + T_{\rm e} + V_{\rm ee}(\mathbf{r}) + V_{\rm NN}(\mathbf{R}) + V_{\rm eN}(\mathbf{r}, \mathbf{R})\right] \Psi(\mathbf{x}, \mathbf{R}) = E\Psi(\mathbf{x}, \mathbf{R}) \tag{2}$$

where $\mathbf{x} \equiv (\mathbf{r}, s)$ is the full collection of position and spin variables. Clearly, an exact solution of Eq. (2) is not possible. The Born-Oppenheimer approximation consists in the recognition that there is a strong separation of time scales between the electronic and nuclear motion, since the electrons are lighter than the nuclei by three orders of magnitude. In order to exploit this fact, we assume a solution of the form

$$\Psi(\mathbf{x}, \mathbf{R}) = \phi(\mathbf{x}, \mathbf{R})\chi(\mathbf{R}) \tag{3}$$

where $\chi(\mathbf{R})$ is a nuclear wavefunction and $\phi(\mathbf{x}, \mathbf{R})$ is an electronic wavefunction that depends parametrically on the nuclear positions. Note that

$$T_{\rm N}\phi(\mathbf{x}, \mathbf{R})\chi(\mathbf{R})$$
$$= \frac{\hbar^2}{2} \sum_{I=1}^{N} \frac{1}{M_I} \left[\phi(\mathbf{x}, \mathbf{R})\nabla_I^2\chi(\mathbf{R}) + \chi(\mathbf{R})\nabla_I^2\phi(\mathbf{x}, \mathbf{R}) + 2\nabla_I\phi(\mathbf{x}, \mathbf{R}) \cdot \nabla_I\chi(\mathbf{R})\right] \tag{4}$$

The Born-Oppenheimer consists in neglecting $\nabla_I\phi(\mathbf{x}, \mathbf{R})$ terms with the justification that the nuclear wavefunction $\chi(\mathbf{R})$ is more localized than the electronic wavefunction, hence, we expect $\nabla_I\chi(\mathbf{R}) \gg \nabla_I\phi(\mathbf{x}, \mathbf{R})$. Substitution of Eq. (3) with the above approximation into Eq. (2) gives

$$\left[T_{\rm e} + V_{\rm ee}(\mathbf{r}) + V_{\rm eN}(\mathbf{r}, \mathbf{R})\right] \phi(\mathbf{x}, \mathbf{R})\chi(\mathbf{R}) + \phi(\mathbf{x}, \mathbf{R})T_{\rm N}\chi(\mathbf{R}) + V_{\rm NN}(\mathbf{R})\phi(\mathbf{x}, \mathbf{R})\chi(\mathbf{R})$$

$$= E\phi(\mathbf{x}, \mathbf{R})\chi(\mathbf{R}) \tag{5}$$

Dividing by $\phi(\mathbf{x}, \mathbf{R})\chi(\mathbf{R})$ then gives:

$$\frac{\left[T_{\rm e} + V_{\rm ee}(\mathbf{r}) + V_{\rm eN}(\mathbf{r}, \mathbf{R})\right] \phi(\mathbf{x}, \mathbf{R})}{\phi(\mathbf{x}, \mathbf{R})} = E - \frac{\left[T_{\rm N} + V_{\rm NN}(\mathbf{R})\right] \chi(\mathbf{R})}{\chi(\mathbf{R})} \tag{6}$$

From the above, it is clear that the left side can only be a function of $\mathbf{R}$ alone. Let this function be denoted, $\varepsilon(\mathbf{R})$. Thus,

$$\frac{\left[T_{\mathrm{e}} + V_{\mathrm{ee}}(\mathbf{r}) + V_{\mathrm{eN}}(\mathbf{r},\mathbf{R})\right]\phi(\mathbf{x},\mathbf{R})}{\phi(\mathbf{x},\mathbf{R})} = \varepsilon(\mathbf{R})$$

$$\left[T_{\mathrm{e}} + V_{\mathrm{ee}}(\mathbf{r}) + V_{\mathrm{eN}}(\mathbf{r},\mathbf{R})\right]\phi(\mathbf{x},\mathbf{R}) = \varepsilon(\mathbf{R})\phi(\mathbf{x},\mathbf{R}) \tag{7}$$

Eq. (7) is an electronic eigenvalue equation for an electronic Hamiltonian, $H_{\mathrm{e}}(\mathbf{R}) = T_{\mathrm{e}} + V_{\mathrm{ee}}(\mathbf{r}) + V_{\mathrm{eN}}(\mathbf{r},\mathbf{R})$ which will yield a set of eigenfunction, $\varphi_n(\mathbf{x},\mathbf{R})$ and eigenvalues, $\varepsilon_n(\mathbf{R})$, which depend parametrically on the nuclear positions, $\mathbf{R}$. For each solution, there will be a nuclear eigenvalue equation:

$$\left[T_{\mathrm{N}} + V_{\mathrm{NN}}(\mathbf{R}) + \varepsilon_n(\mathbf{R})\right]\chi(\mathbf{R}) = E\chi(\mathbf{R}) \tag{8}$$

Moreover, each electronic eigenvalue, $\varepsilon_n(\mathbf{R})$ will give rise to an electronic surface on which the nuclear dynamics described by the time-dependent Schrödinger equation for the time-dependent nuclear wave function $X(\mathbf{R},t)$:

$$\left[T_{\mathrm{N}} + V_{\mathrm{NN}}(\mathbf{R}) + \varepsilon_n(\mathbf{R})\right]X(\mathbf{R},t) = i\hbar\frac{\partial}{\partial t}X(\mathbf{R},t) \tag{9}$$

will evolve. The physical interpretation of Eq. (9) is that the electrons respond instantaneously to the nuclear motion, therefore, it is sufficient to obtain a set of instantaneous electronic eigenvalues and eigenfunctions at each nuclear configuration, $\mathbf{R}$ (hence the parametric dependence of $\varphi_n(\mathbf{x},\mathbf{R})$ and $\varepsilon_n(\mathbf{R})$ on $\mathbf{R}$). The eigenvalues, in turn, give a family of (uncoupled) potential surfaces on which the nuclear wavefunction can evolve. These surfaces can become coupled by so called non-adiabatic effects, contained in the terms that have been neglected in the above derivation.

In many cases, non-adiabatic effects can be neglected, and we may consider motion *only* on the ground electronic surface described by:

$$\left[T_{\mathrm{e}} + V_{\mathrm{ee}}(\mathbf{r}) + V_{\mathrm{eN}}(\mathbf{r},\mathbf{R})\right]\varphi_0(\mathbf{x},\mathbf{R}) = \varepsilon_0(\mathbf{R})\varphi_0(\mathbf{x},\mathbf{R})$$

$$\left[T_{\mathrm{N}} + \varepsilon_0(\mathbf{R}) + V_{\mathrm{NN}}(\mathbf{R})\right]X(\mathbf{R},t) = i\hbar\frac{\partial}{\partial t}X(\mathbf{R},t) \tag{10}$$

Moreover, if nuclear quantum effects can be neglected, then we may arrive at classical nuclear evolution by assuming $X(\mathbf{R},t)$ is of the form

$$X(\mathbf{R},t) = A(\mathbf{R},t)e^{iS(\mathbf{R},t)/\hbar} \tag{11}$$

and neglecting all terms involving $\hbar$, which yields an approximate equation for $S(\mathbf{R},t)$:

$$H_{\mathrm{N}}^{(n)}(\nabla_1 S, ..., \nabla_N S, \mathbf{R}_1, ..., \mathbf{R}_N) + \frac{\partial S}{\partial t} = 0 \tag{12}$$

which is just the classical Hamiltonian-Jacobi equation with

$$H_{\mathrm{N}}^{(n)}(\mathbf{P}_1, ..., \mathbf{P}_N, \mathbf{R}_1, ..., \mathbf{R}_N) = \sum_{I=1}^{N}\frac{\mathbf{P}_I^2}{2M_I} + V_{\mathrm{nn}}(\mathbf{R}) + \varepsilon_n(\mathbf{R}) \tag{13}$$

denoting the classical nuclear Hamiltonian. The Hamilton-Jacobi equation is equivalent to classical motion on the ground-state surface, $E_0(\mathbf{R}) = \varepsilon_0(\mathbf{R}) + V_{\rm NN}(\mathbf{R})$ given by

$$M_I \ddot{\mathbf{R}}_I = -\nabla_I E_0(\mathbf{R}) \tag{14}$$

Note that the force $\nabla_I E_0(\mathbf{R})$ contains a term from the nuclear-nuclear repulsion and a term from the derivative of the electronic eigenvalue, $\varepsilon_0(\mathbf{R})$. Because of the Hellman-Feynman theorem, this term is equivalent to:

$$\nabla_I \varepsilon_0(\mathbf{R}) = \langle \varphi_0(\mathbf{R}) | \nabla_I H_{\rm e}(\mathbf{R}) | \varphi_0(\mathbf{R}) \rangle \tag{15}$$

Finally, we need to specify how the electronic equation is to be solved to obtain the ground state eigenvalue, $\varepsilon_0(\mathbf{R})$. Again, an exact solution to the electronic problem is, in general, not possible. However, a useful approximation is given by the density functional theory, which states, via the Hohenberg-Kohn theorem, that the ground state energy, $\varepsilon_0(\mathbf{R})$ at a given nuclear configuration, $\mathbf{R}$ is obtained by minimizing a certain functional, $\varepsilon[n]$, over all electronic densities

$$n(\mathbf{r}) = \sum_{s, s_2, ..., s_{N_e}} \int d\mathbf{r}_2 \cdots d\mathbf{r}_{N_e} \, |\varphi_0(\mathbf{r}, s, \mathbf{r}_2, s_2, ..., \mathbf{r}_{N_e}, s_{N_e})|^2 \tag{16}$$

(Here, $\mathbf{r}$ and s represent a single position and spin variable, respectively.) A convenient form for this functional is given by the scheme of Kohn and Sham, in which a set of doubly occupied single-particle states, $\psi_i(\mathbf{r})$, $i = 1, ..., N_e/2$, each containing a spin-up and a spin-down electron, is introduced. These are known as the Kohn-Sham (KS) orbitals. In terms of these orbitals, the density is given by

$$n(\mathbf{r}) = \sum_i |\psi_i(\mathbf{r})|^2 \tag{17}$$

and the functional takes the form

$$\varepsilon[\{\psi_i\}] = -\frac{\hbar^2}{2m} \sum_i \langle \psi_i | \nabla^2 | \psi_i \rangle + \frac{e^2}{2} \int d\mathbf{r} \, d\mathbf{r}' \frac{n(\mathbf{r}) n(\mathbf{r}')}{|\mathbf{r} - \mathbf{r}'|} + \varepsilon_{\rm xc}[n] + \int d\mathbf{r} \, n(\mathbf{r}) V_{\rm en}(\mathbf{r}, \mathbf{R}) \tag{18}$$

The first term in the functional represents the quantum kinetic energy, the second is the direct Coulomb term from Hartree-Fock theory, the third term is the exact (unknown) exchange and correlation energies, and the fourth term is the interaction of the electron density with the external potential due to the nuclei. This functional is minimized over the set of single-particle orbitals subject to an orthogonality condition

$$\langle \psi_i | \psi_j \rangle = \delta_{ij} \tag{19}$$

Moreover, in order to combine this minimization with the nuclear dynamics of Eq. (14), it is necessary to carry out the minimization at each nuclear configuration. Thus, if Eq. (14) is integrated in a MD calculation using a numerical integrator, then the minimization would need to be carried out at each step of the MD simulation and the forces computed using the orbitals thus obtained.

In 1985, Car and Parrinello showed that this coupling between nuclear time evolution and electronic minimization could be treated efficiently via an implicit adiabatic dynamics approach[1]. In their scheme, a fictitious dynamics for the electronic orbitals is invented which, given orbitals initially at the minimum for an initial nuclear configuration, would

allow them to follow the nuclear motion adiabatically, and thus, be automatically at their approximately minimized configuration at each step of the MD evolution. This dynamics is controlled by introducing a set of orbitals "velocities" $\{\dot{\psi}_i(\mathbf{r})\}$ and a fictitious electronic "kinetic energy" (not to be confused with the true quantum kinetic energy) given by

$$K_{\rm fict} = \mu \sum_i \langle \dot{\psi}_i | \dot{\psi}_i \rangle \tag{20}$$

where μ is a fictitious mass parameter (having units of energy$\times$time^2) that controls the time scale on which the electrons "evolve" and introducing a Lagrangian that includes the orbitals as fictitious dynamical degrees of freedom:

$$L = \mu \sum_i \langle \dot{\psi}_i | \dot{\psi}_i \rangle + \frac{1}{2} \sum_{I=1}^{N} M_I \dot{\mathbf{R}}_I^2 - E[\{\psi\}, \mathbf{R}] + \sum_{i,j} \left[\Lambda_{ij} \left(\langle \psi_i | \psi_j \rangle - \delta_{ij} \right) \right] \tag{21}$$

where $E[\{\psi\}, \mathbf{R}] = \varepsilon[\{\psi\}, \mathbf{R}] + V_{\rm nn}(\mathbf{R})$. The matrix Λ_{ij} is a set of Lagrange multipliers introduced in order to ensure that the condition $\langle \psi_i | \psi_j \rangle = \delta_{ij}$ is satisfied dynamically as a constraint. The Euler-Lagrange equations

$$\frac{d}{dt} \left(\frac{\delta L}{\delta \dot{\psi}_i^*(\mathbf{r})} \right) - \frac{\delta L}{\delta \psi_i^*(\mathbf{r})} = 0$$

$$\frac{d}{dt} \left(\frac{\partial L}{\partial \dot{\mathbf{R}}_I} \right) - \frac{\partial L}{\partial \mathbf{R}_I} = 0 \tag{22}$$

gives the following coupled dynamical equations of motion:

$$\begin{aligned} M_I \ddot{\mathbf{R}}_I &= -\nabla_I E[\{\psi\}, \mathbf{R}] \\ \mu \ddot{\psi}_i(\mathbf{r}) &= -\frac{\delta}{\delta \psi_i^*(\mathbf{r})} E[\{\psi\}, \mathbf{R}] + \sum_j \Lambda_j \psi_j(\mathbf{r}) \end{aligned} \tag{23}$$

These are known as the Car-Parrinello (CP) equations, and they form the basis of the AIMD method. The electronic equation can also be written in an abstract bra-ket form as:

$$\mu |\ddot{\psi}_i\rangle = -\frac{\partial E}{\partial \langle \psi_i |} + \sum_j \Lambda_{ij} |\psi_j\rangle \tag{24}$$

Below, we present an algorithm for integrating the CP equations subject to the orthogonality constraint based on the velocity Verlet scheme derived from the Liouville operator formalism in the path integral MD lecture[32].

Beginning with an initially minimized set of Kohn-Sham orbitals, $\{|\psi_i(0)\rangle\}$ corresponding to an initial nuclear configuration, $\mathbf{R}(0)$ and initial velocities, $\{\dot{\psi}_i(0)\rangle\}$, $\dot{\mathbf{R}}(0)$, the first step is a velocity update:

$$\begin{aligned} |\dot{\psi}_i^{(1)}(0)\rangle &= |\dot{\psi}_i(0)\rangle + \frac{\Delta t}{2\mu} |\varphi_i(0)\rangle \qquad i = 1, ..., \frac{N_e}{2} \\ \dot{\mathbf{R}}_I(\Delta t/2) &= \dot{\mathbf{R}}_I(0) + \frac{\Delta t}{2M_I} \mathbf{F}_I(0) \qquad I = 1, ..., N \end{aligned} \tag{25}$$

followed by a position/orbital update:

$$|\tilde{\psi}_i\rangle = |\psi_i(0)\rangle + \Delta t|\dot{\psi}_i^{(1)}\rangle \qquad i = 1, ..., \frac{N_e}{2}$$

$$\mathbf{R}_I(\Delta t) = \mathbf{R}_I(0) + \Delta t\dot{\mathbf{R}}_I(\Delta t/2) \qquad I = 1, ..., N \tag{26}$$

where $|\varphi_i(0)\rangle = (\partial E/\partial\langle\psi_i|)|_{t=0}$ is the initial force on the orbital, $|\psi_i\rangle$. At this point, we do not yet have the orbitals at $t = \Delta t$ or orbital velocities at $t = \Delta t/2$ because the constraint force $\Lambda_{ij}|\psi_j\rangle$ needs to be applied to both the orbitals and orbital velocities. In order to do this, we need to determine the Lagrange multiplier matrix, which is accomplished by enforcing the orthogonality constraint on the orbitals at $t = \Delta t$:

$$\langle\psi_i(\Delta t)|\psi_j(\Delta t)\rangle = \delta_{ij} \tag{27}$$

where

$$|\psi_i(\Delta t)\rangle = |\tilde{\psi}_i\rangle + \sum_j X_{ij}|\psi_j(0)\rangle \tag{28}$$

where $X_{ij} = (\Delta t^2/2\mu)\Lambda_{ij}$. Substituting Eq. (28) into Eq. (27) yields a matrix equation for the Lagrange multipliers:

$$\mathrm{XX}^\dagger + \mathrm{XB} + \mathrm{B}^\dagger\mathrm{X}^\dagger + \mathrm{A} = \mathrm{I} \tag{29}$$

where $A_{ij} = \langle\tilde{\psi}_i|\tilde{\psi}_j\rangle$ and $B_{ij} = \langle\psi_i(0)|\tilde{\psi}_j\rangle$. Noting that $\mathrm{A} = I + \mathcal{O}(\Delta t^2)$ and $\mathrm{B} = I + \mathcal{O}(\Delta t)$, the matrix equation can be solved iteratively via

$$\mathrm{X}_{n+1} = \frac{1}{2}\left[\mathrm{I} - \mathrm{A} + \mathrm{X}_n(\mathrm{I} - \mathrm{B}) + (I - \mathrm{B}^\dagger)X_n^\dagger - \mathrm{X}_n^2\right] \tag{30}$$

starting from an initial guess

$$\mathrm{X}_0 = \frac{1}{2}(\mathrm{I} - \mathrm{A}) \tag{31}$$

Once the matrix X_{ij} is obtained, the orbitals are updated using Eq. (28) and an orbital velocity update

$$|\dot{\psi}_i^{(2)}\rangle = |\dot{\psi}_i^{(1)}\rangle + \frac{1}{\Delta t}\sum_j X_{ij}|\psi_j(0)\rangle \tag{32}$$

is performed.

At this point, the new orbitals and nuclear forces, $|\varphi_i(\Delta t)\rangle$ and $\mathbf{F}_I(\Delta t)$ are calculated, and a velocity update of the form

$$|\dot{\psi}_i^{(3)}\rangle = |\dot{\psi}_i^{(2)}\rangle + \frac{\Delta t}{2\mu}|\varphi_i(\Delta t)\rangle \qquad i = 1, ..., \frac{N_e}{2}$$

$$\dot{\mathbf{R}}_I(\Delta t) = \dot{\mathbf{R}}_I(\Delta t/2) + \frac{\Delta t}{2M_I}\mathbf{F}_I(\Delta t) \tag{33}$$

is performed. Again, we do not have the final orbital velocities until an appropriate constraint force is applied. For the velocities, the appropriate force is the first time derivative of the orthogonality constraint:

$$\langle\psi_i(\Delta t)|\dot{\psi}_j(\Delta t)\rangle + \langle\dot{\psi}_i(\Delta t)|\psi_j(\Delta t)\rangle = 0 \tag{34}$$

where

$$|\dot{\psi}_i(\Delta t)\rangle = |\dot{\psi}_i^{(3)}\rangle + \sum_j Y_{ij}|\psi_i(\Delta t)\rangle \tag{35}$$

and Y_{ij} are a new set of Lagrange multipliers for enforcing the condition Eq. (34). Substituting Eq. (35) into Eq. (34) gives a simple solution for Y_{ij}:

$$\mathrm{Y} = -\frac{1}{2}\left(\mathrm{C} + \mathrm{C}^\dagger\right) \tag{36}$$

where $C_{ij} = \langle\psi_i(\Delta t)|\dot{\psi}_i^{(3)}\rangle$. Given the matrix, Y_{ij}, the final orbital velocities are obtained via Eq. (35).

3 Plane Wave Basis Sets

In the traditional CP approach, periodic boundary conditions are employed, and the orbitals, $\{\psi_i(\mathbf{r})\}$ become Bloch functions, $\{\psi_{i\mathbf{k}}(\mathbf{r})\}$, where $\mathbf{k}$ samples the first Brioullin zone. These Bloch functions are expanded in a plane wave basis:

$$\psi_{i\mathbf{k}}(\mathbf{r}) = \frac{1}{\sqrt{\Omega}} e^{i\mathbf{k}\cdot\mathbf{r}} \sum_{\mathbf{g}} c_{\mathbf{g}}^{i\mathbf{k}} e^{i\mathbf{g}\cdot\mathbf{r}} \tag{37}$$

where $c_{\mathbf{g}}^{i\mathbf{k}}$ is a set of expansion coefficients, Ω is the system volume, $\mathbf{g} = 2\pi\mathbf{h}^{-1}\hat{\mathbf{g}}$ is a reciprocal lattice vector, $\mathbf{h}$ is the cell matrix whose columns are the cell vectors, and $\hat{\mathbf{g}}$ is a vector of integers. An advantage of plane waves is that the sums needed to go back and forth between reciprocal space and real space can be performed efficiencly using fast Fourier transforms (FFTs). For the applications to be considered herein, which are largely concerned with nonmetallic systems, it is sufficient to consider only the Γ-point ($\mathbf{k} = (0,0,0)$), so that the plane wave expansion becomes

$$\psi_i(\mathbf{r}) = \frac{1}{\sqrt{\Omega}} \sum_{\mathbf{g}} c_{\mathbf{g}}^{i} e^{i\mathbf{g}\cdot\mathbf{r}} \tag{38}$$

In this case, the coefficients become dynamical variables, and the CP equations take the form:

$$\begin{aligned} M_I\ddot{\mathbf{R}}_I &= -\frac{\partial E}{\partial \mathbf{R}_I} \\ \mu\ddot{c}_{\mathbf{g}}^{i} &= -\frac{\partial E}{\partial c_{\mathbf{g}}^{i*}} + \sum_j \Lambda_{ij} c_{\mathbf{g}}^{j} \end{aligned} \tag{39}$$

At the Γ-point, the orbitals can always be chosen to be real functions. Therefore, the plane-wave expansion coefficients satisfy the following property

$$c_{\mathbf{g}}^{i*} = c_{-\mathbf{g}}^{i} \tag{40}$$

which requires keeping only half of the full set of plane-wave expansion coefficients. In actual applications, plane waves up to a given cutoff, $|\mathbf{g}|^2/2 < E_{\mathrm{cut}}$, only are kept. Similarly, the density $n(\mathbf{r})$ given by Eq. (17) can also be expanded in a plane wave basis:

$$n(\mathbf{r}) = \frac{1}{\Omega} \sum_{\mathbf{g}} n_{\mathbf{g}} e^{i\mathbf{g}\cdot\mathbf{r}} \tag{41}$$

However, since $n(\mathbf{r})$ is obtained as a square of the KS orbitals, the cutoff needed for this expansion is $4E_{\rm cut}$ for consistency with the orbital expansion.

Using Eqs. (37) and (41) and the orthogonality of the plane waves, it is straightforward to compute the various energy terms. For example, the kinetic energy can be easily shown to be

$$\varepsilon_{\rm KE} = -\frac{1}{2}\sum_i \int d\mathbf{r}\ \psi_i^*(\mathbf{r})\nabla^2\psi_i(\mathbf{r}) = \frac{1}{2}\sum_i\sum_{\mathbf{g}} g^2|c_{\mathbf{g}}^i|^2 \tag{42}$$

where $g = |\mathbf{g}|$. Similarly, the Hartree energy becomes

$$\varepsilon_{\rm H} = \frac{1}{2}\int d\mathbf{r}\ d\mathbf{r}'\ \frac{n(\mathbf{r})n(\mathbf{r}')}{|\mathbf{r}-\mathbf{r}'|} = \frac{1}{\Omega}{\sum_{\mathbf{g}}}' \frac{4\pi}{g^2}|n_{\mathbf{g}}|^2 \tag{43}$$

where the summation excludes the $\mathbf{g} = (0,0,0)$ term.

The exchange and correlation energy, $\varepsilon_{\rm xc}[n]$ is generally treated within a local density (LDA) or generalized gradient approximations (GGA) wherein it is assumed to take the approximate form

$$\varepsilon_{\rm xc}[n] \approx \int d\mathbf{r}\ f(n(\mathbf{r}), \nabla n(\mathbf{r}), \nabla^2 n(\mathbf{r})) = \frac{\Omega}{N_{\rm grid}}\sum_{\mathbf{r}} f(n(\mathbf{r}), \nabla n(\mathbf{r}), \nabla^2 n(\mathbf{r})) \tag{44}$$

where the sum is taken over a set of $N_{\rm grid}$ real-space grid points. The gradient and (if needed) the Laplacian of the density can be computed efficiently using FFTs:

$$\begin{aligned}\nabla n(\mathbf{r}) &= \sum_{\mathbf{g}} i\mathbf{g}e^{i\mathbf{g}\cdot\mathbf{r}}\sum_{\mathbf{r}'} n(\mathbf{r}')e^{-i\mathbf{g}\cdot\mathbf{r}'} \\ \nabla^2 n(\mathbf{r}) &= -\sum_{\mathbf{g}} g^2 e^{i\mathbf{g}\cdot\mathbf{r}}\sum_{\mathbf{r}'} n(\mathbf{r}')e^{-i\mathbf{g}\cdot\mathbf{r}'}\end{aligned} \tag{45}$$

The external energy is made somewhat complicated by the fact that, in a plane wave basis, very large basis sets are needed to treat the rapid spatial fluctuations of core electrons. Therefore, core electrons are often replaced by atomic pseudopotentials[23–25] are augmented plane wave techniques[26]. Here, we shall discuss the former. In the atomic pseudopotential scheme, the nucleus plus the core electrons are treated in a frozen core type approximation as an ion carrying only the valence charge. In order to make this approximation, the valence orbitals, which, in principle must be orthogonal to the core orbitals, must see a different pseudopotential for each angular momentum component in the core, which means that the pseudopotential must be nonlocal. To see how this comes about, we consider a potential operator of the form

$$\hat{V}_{\rm pseud} = \sum_{l=0}^{\infty}\sum_{m=-l}^{l} v_l(r)|lm\rangle\langle lm| \tag{46}$$

where r is the distance from the ion, and $|lm\rangle\langle lm|$ is a projection operator onto each angular momentum component. In order to truncate the infinite sum over l in Eq. (46), we assume that for some $l \geq \bar{l}$, $v_l(r) = v_{\bar{l}}(r)$ and add and subtract the function $v_{\bar{l}}(r)$ in Eq.

(46):

$$\hat{V}_{\rm pseud} = \sum_{l=0}^{\infty}\sum_{m=-l}^{l}(v_l(r)-v_{\bar{l}}(r))|lm\rangle\langle lm| + v_{\bar{l}}(r)\sum_{l=0}^{\infty}\sum_{m=-l}^{l}|lm\rangle\langle lm|$$

$$= \sum_{l=0}^{\infty}\sum_{m=-l}^{l}(v_l(r)-v_{\bar{l}}(r))|lm\rangle\langle lm| + v_{\bar{l}}(r)$$

$$\approx \sum_{l=0}^{\bar{l}-1}\sum_{m=-l}^{l}\Delta v_l(r)|lm\rangle\langle lm| \qquad (47)$$

where the second line follows from the fact that the sum of the projection operators is unity, $\Delta v_l(r) = v_l(r) - v_{\bar{l}}(r)$, and the sum in the third line is truncated before $\Delta v_l(r) = 0$. The complete pseudopotential operator will be

$$\hat{V}_{\rm pseud}(r;\mathbf{R}_1,...,\mathbf{R}_N) = \sum_{I=1}^{N}\left[v_{\rm loc}(|\mathbf{r}-\mathbf{R}_I|) + \sum_{l=0}^{\bar{l}-1}\Delta v_l(|\mathbf{r}-\mathbf{R}_I|)|lm\rangle\langle lm|\right] \qquad (48)$$

where $v_{\rm loc}(r) \equiv v_{\bar{l}}(r)$ is known as the local part of the pseudopotential (having no projection operator attached to it). Now, the external energy, being derived from the ground-state expectation value of a one-body operator, will be given by

$$\varepsilon_{\rm ext} = \sum_i \langle\psi_i|\hat{V}_{\rm pseud}|\psi_i\rangle \qquad (49)$$

The first (local) term gives simply a local energy of the form

$$\varepsilon_{\rm loc} = \sum_{I=1}^{N}\int d\mathbf{r}\; n(\mathbf{r})v_{\rm loc}(|\mathbf{r}-\mathbf{R}_I|) \qquad (50)$$

which can be evaluated in reciprocal space as

$$\varepsilon_{\rm loc} = \frac{1}{\Omega}\sum_{I=1}^{N}\sum_{\mathbf{g}} n^*_{\mathbf{g}}\tilde{v}_{\rm loc}(\mathbf{g})e^{-i\mathbf{g}\cdot\mathbf{R}_I} \qquad (51)$$

where $\tilde{V}_{\rm loc}(\mathbf{g})$ is the Fourier transform of the local potential. Note that at $\mathbf{g} = (0,0,0)$, only the nonsingular part of $\tilde{v}_{\rm loc}(\mathbf{g})$ contributes. In the evaluation of the local term, it is often convenient to add and subtract a long-range term of the form $Z_I{\rm erf}(\alpha_I r)/r$, where ${\rm erf}(x)$ is the error function, for each ion in order to obtain the nonsingular part explicitly and a residual short-range function $\bar{v}_{\rm loc}(|\mathbf{r}-\mathbf{R}_I|) = v_{\rm loc}(|\mathbf{r}-\mathbf{R}_I|) - Z_I{\rm erf}(\alpha_I|\mathbf{r}-\mathbf{R}_I|)/|\mathbf{r}-\mathbf{R}_I|$ for each ionic core. For the nonlocal contribution, Eq. (38) is substituted into Eq. (48), an expansion of the plane waves in terms of spherical Bessel functions and spherical harmonics is made, and, after some algebra, one obtains

$$\varepsilon_{\rm NL} = \sum_i\sum_I\sum_{\mathbf{g},\mathbf{g}'} e^{-i\mathbf{g}\cdot\mathbf{R}_I}c^{i^*}_{\mathbf{g}}v_{\rm NL}(\mathbf{g},\mathbf{g}')c^i_{\mathbf{g}'}e^{i\mathbf{g}'\cdot\mathbf{R}_I} \qquad (52)$$

where

$$v_{\rm NL}(\mathbf{g},\mathbf{g}') = (4\pi)^2 \sum_{l=0}^{\bar{l}-1} \sum_{m=-l}^{l} \int dr\ r^2\ j_l(gr) j_l(g'r) \Delta v_l(\mathbf{r}) Y_{lm}(\theta_{\mathbf{g}},\phi_{\mathbf{g}}) Y^*_{lm}(\theta_{\mathbf{g}'},\phi_{\mathbf{g}'}) \tag{53}$$

where $\theta_{\mathbf{g}}$ and $\phi_{\mathbf{g}}$ are the spherical polar angles associated with the vector $\mathbf{g}$, and same for $\theta_{\mathbf{g}'}$ and $\phi_{\mathbf{g}'}$. Eq. (53) shows that the evaluation of the nonlocal energy can be quite computationally expensive. It also shows, however, that the matrix element is *almost* separable in $\mathbf{g}$ and $\mathbf{g}'$ dependent terms. A fully separable approximation can be obtained by writing

$$v_{\rm NL}(\mathbf{g},\mathbf{g}') = (4\pi)^2 \sum_{l=0}^{\bar{l}-1} \sum_{m=-l}^{l} \int dr\ r^2 \int dr'\ r'^2 j_l(gr) j_l(g'r') \Delta v_l(\mathbf{r}) \frac{\delta(r-r')}{rr'}$$

$$\times\ Y_{lm}(\theta_{\mathbf{g}},\phi_{\mathbf{g}}) Y^*_{lm}(\theta_{\mathbf{g}'},\phi_{\mathbf{g}'}) \tag{54}$$

where a radial δ-function has been introduced. Now, the δ-function is expanded in terms of a set of radial eigenfunctions (usually taken to be those of the Hamiltonian from which the pseudopotential is obtained) for each angular momentum channel

$$\frac{\delta(r-r')}{rr'} = \sum_{n=0}^{\infty} \phi^*_{nl}(r) \phi_{nl}(r') \tag{55}$$

If this expansion is now substituted into Eq. (54), the result is

$$v_{\rm NL}(\mathbf{g},\mathbf{g}') = (4\pi)^2 \sum_{n=0}^{\infty} \sum_{l=0}^{\bar{l}-1} \sum_{m=-l}^{l} \left[\int dr\ r^2\ j_l(gr) \Delta v_l(\mathbf{r}) \phi^*_{nl}(r) Y_{lm}(\theta_{\mathbf{g}},\phi_{\mathbf{g}}) \right]$$

$$\times \left[\int dr'\ r'^2 j_l(g'r') Y^*_{lm}(\theta_{\mathbf{g}'},\phi_{\mathbf{g}'}) \phi_{nl}(r') \right] \tag{56}$$

which is now fully separable at the expense of another infinite sum that needs to be truncated. Although the sum over n can be truncated after any number of terms, the so called *Kleinman-Bylander approximation*[27] is the result of truncating it at just a single term. The result of this truncation can be shown to yield the approximation form:

$$v_{\rm NL}(\mathbf{g},\mathbf{g}') \approx (4\pi)^2 \sum_{l=0}^{\bar{l}-1} \sum_{m=-l}^{l} N^{-1}_{lm} \left[\int dr\ r^2\ j_l(gr) \Delta v_l(\mathbf{r}) \phi^*_l(r) Y_{lm}(\theta_{\mathbf{g}},\phi_{\mathbf{g}}) \right]$$

$$\times \left[\int dr'\ r'^2 \Delta v_l(r') j_l(g'r') Y^*_{lm}(\theta_{\mathbf{g}'},\phi_{\mathbf{g}'}) \phi_l(r') \right] \tag{57}$$

where

$$N_{lm} = \int dr\ r^2\ \phi^*_l(r) \Delta v_l(r) \phi_l(r) \tag{58}$$

and $\phi_l(r) \equiv \phi_{0l}(r)$. Finally, substituting Eq. (57) into Eq. (52) gives the nonlocal energy as

$$\varepsilon_{\rm NL} = \sum_{i=1}^{N_e} \sum_{I=1}^{N} \sum_{l=0}^{\bar{l}-1} \sum_{m=-l}^{l} Z^*_{iIlm} Z_{iIlm} \tag{59}$$

where

$$Z_{iIlm} = \sum_{\mathbf{g}} c^i_{\mathbf{g}} e^{i\mathbf{g}\cdot\mathbf{R}_I} \tilde{F}_{lm}(\mathbf{g}) \tag{60}$$

and

$$\tilde{F}_{lm}(\mathbf{g}) = 4\pi N_{lm}^{-1/2} \int dr\ r^2 j_l(gr) \Delta v_l(ur) \phi_l(r) Y_{lm}(\theta_{\mathbf{g}}, \phi_{\mathbf{g}}) \tag{61}$$

Having specified all of the energy terms in terms of the plane wave expansion, these expressions can be differentiated in order to obtain the forces on the ions and coefficients needed for the CP equations of motion.

The last issue on which we shall touch briefly is that of boundary conditions within the plane wave description. Plane waves naturally describe a situation in which three-dimensional periodic boundary conditions are to be used, such as in solids and liquids. What if we wish to treat systems, such as cluster, surface, or wire, in which one or more boundaries is *not* periodic? It turns out that such situations can be treated rather easily within the plane wave description using a technique developed by Martyna and Tuckerman[28,29], which involves the use of a screening function in the long-range energy terms, i.e. the Hartree and local pseudopotential terms. The idea is to use the so called first image form of the average energy in order to form an approximation to a cluster, wire, or surface system, whose error can be controlled by the dimensions of the simulation cell. Thus, given any density, $n(\mathbf{r})$ and any interaction potential, $\phi(\mathbf{r}-\mathbf{r}')$, the average potential energy in this approximation is given by

$$\langle\phi\rangle^{(1)} = \frac{1}{2\Omega} \sum_{\mathbf{g}} |n_{\mathbf{g}}|^2 \bar{\phi}(-\mathbf{g}) \tag{62}$$

where $\bar{\phi}(\mathbf{g})$ is a Fourier expansion coefficient of the potential given by

$$\begin{aligned}
\bar{\phi}(\mathbf{g}) &= \int_{-L_c/2}^{L_c/2} dz \int_{-L_b/2}^{L_b/2} dy \int_{-L_a/2}^{L_a/2} dx\ \phi(\mathbf{r}) e^{-i\mathbf{g}\cdot\mathbf{r}} \qquad \text{(Cluster)} \\
\bar{\phi}(\mathbf{g}) &= \int_{-L_c/2}^{L_c/2} dz \int_{-L_b/2}^{L_b/2} dy \int_{-\infty}^{\infty} dx\ \phi(\mathbf{r}) e^{-i\mathbf{g}\cdot\mathbf{r}} \qquad \text{(Wire)} \\
\bar{\phi}(\mathbf{g}) &= \int_{-L_c/2}^{L_c/2} dz \int_{-\infty}^{\infty} dy \int_{-\infty}^{\infty} dx\ \phi(\mathbf{r}) e^{-i\mathbf{g}\cdot\mathbf{r}} \qquad \text{(Surface)}
\end{aligned} \tag{63}$$

Here, L_a, L_b, and L_c are the dimensions of the simulation cell (assumed to be orthorhombic for simplicity) in the x, y, and z directions. In order to have an expression that is easily computed within the plane wave description, consider two functions $\phi^{(\mathrm{long})}(\mathbf{r})$ and $\phi^{(\mathrm{short})}(\mathbf{r})$, which are assumed to the long and short range contributions to the total potential, such that

$$\phi(\mathbf{r}) = \phi^{(\mathrm{long})}(\mathbf{r}) + \phi^{(\mathrm{short})}(\mathbf{r})$$

$$\bar{\phi}(\mathbf{g}) = \bar{\phi}^{(\mathrm{long})}(\mathbf{g}) + \bar{\phi}^{(\mathrm{short})}(\mathbf{g}). \tag{64}$$

We require that $\phi^{(\mathrm{short})}(\mathbf{r})$ vanish exponentially quickly at large distances from the center of the parallelepiped and that $\phi^{(\mathrm{long})}(\mathbf{r})$ contain the long range dependence of the full

potential, $\phi(\mathbf{r})$. With these two requirements, it is possible to write

$$\begin{aligned}\bar{\phi}^{(\text{short})}(\mathbf{g}) &= \int_{D(\Omega)} d\mathbf{r}\ \exp(-i\mathbf{g}\cdot\mathbf{r})\phi^{(\text{short})}(\mathbf{r}) \\ &= \int_{\text{all space}} d\mathbf{r}\exp(-i\mathbf{g}\cdot\mathbf{r})\phi^{(\text{short})}(\mathbf{r}) + \epsilon(\mathbf{g}) \\ &= \tilde{\phi}^{(\text{short})}(\mathbf{g}) + \epsilon(\mathbf{g}) \end{aligned} \tag{65}$$

with exponentially small error, $\epsilon(\mathbf{g})$, provided the range of $\phi^{(\text{short})}(\mathbf{r})$ is chosen small compared size of the parallelepiped, i.e. Eq. (65) defines the properties that the heretofore arbitrary function, $\phi^{(\text{short})}(\mathbf{r})$, must satisfy. Therefore, $\phi^{(\text{short})}(\mathbf{r})$, will be made a function of a convergence parameter, α, which can be used to adjust the range of $\phi^{(\text{short})}(\mathbf{r})$ such that $\epsilon(\mathbf{g}) \sim 0$ and the error, $\epsilon(\mathbf{g})$, will be neglected in the following.

The function, $\tilde{\phi}^{(\text{short})}(\mathbf{g})$, is the Fourier transform of $\phi^{(\text{short})}(\mathbf{r})$ evaluated at the quantized g-vector. Therefore,

$$\begin{aligned}\bar{\phi}(\mathbf{g}) &= \bar{\phi}^{(\text{long})}(\mathbf{g}) + \tilde{\phi}^{(\text{short})}(\mathbf{g}) \\ &= \bar{\phi}^{(\text{long})}(\mathbf{g}) - \tilde{\phi}^{(\text{long})}(\mathbf{g}) + \tilde{\phi}^{(\text{short})}(\mathbf{g}) + \tilde{\phi}^{(\text{long})}(\mathbf{g}) \\ &= \hat{\phi}^{(\text{screen})}(\mathbf{g}) + \tilde{\phi}(\mathbf{g}) \end{aligned} \tag{66}$$

where $\tilde{\phi}(\mathbf{g}) = \tilde{\phi}^{(\text{short})}(\mathbf{g}) + \tilde{\phi}^{(\text{long})}(\mathbf{g})$ is the Fourier transform of the full potential, $\phi(\mathbf{r}) = \phi^{(\text{short})}(\mathbf{r}) + \phi^{(\text{long})}(\mathbf{r})$, evaluated at the quantized g-vector and

$$\hat{\phi}^{(\text{screen})}(\mathbf{g}) = \bar{\phi}^{(\text{long})}(\mathbf{g}) - \tilde{\phi}^{(\text{long})}(\mathbf{g}). \tag{67}$$

This result, Eqs. (67) and Eqs. (66), leads to

$$\langle\phi\rangle = \frac{1}{2\Omega}\sum_{\hat{\mathbf{g}}} |\bar{n}(\mathbf{g})|^2 \left[\tilde{\phi}(-\mathbf{g}) + \hat{\phi}^{(\text{screen})}(-\mathbf{g})\right] \tag{68}$$

The new function appearing in the average potential energy, Eq. (68), is the difference between the Fourier series and Fourier transform form of the long range part of the potential energy evaluated at the quantized g-vector (cf Eq.(67)) and will be referred to as the screening function because it is constructed to "screen" the interaction of the system with an infinite array of periodic images. The specific case of the Coulomb potential,

$$\phi(\mathbf{r}) = \frac{1}{r} \tag{69}$$

can be separated into short and long range components via

$$\frac{1}{r} = \frac{\text{erf}(\alpha r)}{r} + \frac{\text{erfc}(\alpha r)}{r} \tag{70}$$

where the first term is long range. Here, α is an arbitrary convergence parameter. The screening function for the cluster case is easily computed by introducing an FFT grid and performing the integration numerically. For the wire and surface cases, analytical expressions can be worked out and are given by

$$\begin{aligned}\bar{\phi}^{(\mathrm{screen})}(\mathbf{g}) =& \frac{4\pi}{g^2} e^{-g^2/4\alpha^2} - \frac{4\pi}{g^2}\left\{\cos\left(\frac{g_c L_c}{2}\right)\right. \\ & \times\left[\exp\left(-\frac{g_s L_c}{2}\right) - \frac{1}{2}\exp\left(-\frac{g_s L_c}{2}\right)\mathrm{erfc}\left(\frac{\alpha^2 L_c - g_s}{2\alpha}\right)\right. \\ & \left.-\frac{1}{2}\exp\left(\frac{g_s L_c}{2}\right)\mathrm{erfc}\left(\frac{\alpha^2 L_c + g_s}{2\alpha}\right)\right] \\ & \left.+\exp\left(-\frac{g^2}{4\alpha^2}\right) Re\left[\mathrm{erfc}\left(\frac{\alpha^2 L_c + i g_c}{2\alpha}\right)\right]\right\} - \frac{4\pi}{g^2} e^{-g^2/4\alpha^2}\end{aligned} \tag{71}$$

(Surface)

$$\begin{aligned}\bar{\phi}^{(\mathrm{screen,Coul})}(\mathbf{g}) =& \frac{4\pi}{g^2}\left[\exp\left(-g^2/4\alpha^2\right) E(\alpha, L_b, g_b) E(\alpha, L_c, g_c)\right. \\ & + \cos\left(\frac{g_b L_b}{2}\right)\frac{4\sqrt{\pi}}{\alpha L_b}\exp\left(-g_c^2/4\alpha^2\right) I(\alpha, L_b, L_c, g_c) \\ & \left.+ \cos\left(\frac{g_c L_c}{2}\right)\frac{4\sqrt{\pi}}{\alpha L_c}\exp\left(-g_b^2/4\alpha^2\right) I(\alpha, L_c, L_b, g_b)\right] \\ & - \frac{4\pi}{g^2} e^{-g^2/4\alpha^2}\end{aligned} \tag{72}$$

(Wire)

where

$$I(\alpha, L_1, L_2, g) = \int_0^{\alpha L_1/2} dx\; x e^{-g_a^2 L_1^2/16x^2} e^{-x^2} E\left(\frac{2x}{L_1}, L_2, g\right) \tag{73}$$

and

$$E(\lambda, L, g) = \mathrm{erf}\left(\frac{\lambda^2 L + ig}{2\lambda}\right) \tag{74}$$

where $\mathbf{g} = (g_a, g_b, g_c)$ and $g_s = \sqrt{g_a^2 + g_b^2}$. The one-dimensional integrals in Eq. (73) are well suited to be performed by Gaussian quadrature techniques.

4 The Path Integral Born-Oppenheimer Approximation and *Ab Initio* Path Integral Molecular Dynamics

The Born-Oppenheimer approximation described above can be recast in terms of imaginary time path integrals. Using the continuous notation previously introduced, the partition function can be written as

$$\begin{aligned}Z(N,V,T) =& \oint \mathcal{D}\mathbf{R}(\tau) \oint \mathcal{D}\mathbf{r}(\tau) \\ & \times \exp\left\{-\frac{1}{\hbar}\int_0^{\beta\hbar} d\tau \left[T_{\mathrm{N}}(\dot{\mathbf{R}}(\tau) + T_{\mathrm{e}}(\dot{\mathbf{r}}(\tau)) + V_{\mathrm{ee}}(\mathbf{r}(\tau)) + V_{\mathrm{NN}}(\mathbf{R}(\tau)) + V_{\mathrm{eN}}(\mathbf{r}(\tau), \mathbf{R}(\tau))\right]\right\}\end{aligned} \tag{75}$$

If the above path integral is approached using the idea of influence functionals[30], then Eq. (75) is written as

$$Z(N,V,T) = \oint \mathcal{D}\mathbf{R}(\tau)\ \exp\left\{-\frac{1}{\hbar}\int_0^{\beta\hbar}\left[T_{\mathrm{N}}(\dot{\mathbf{R}}(\tau)) + V_{\mathrm{NN}}(\mathbf{R}(\tau))\right]\right\} F[\mathbf{R}(\tau)]$$

$$F[\mathbf{R}(\tau)] = \oint \mathcal{D}\mathbf{r}(\tau)\ \exp\left\{-\frac{1}{\hbar}\int_0^{\beta\hbar}\left[T_{\mathrm{e}}(\dot{\mathbf{r}}(\tau)) + V_{\mathrm{ee}}(\mathbf{r}(\tau)) + V_{\mathrm{eN}}(\mathbf{r}(\tau),\mathbf{R}(\tau))\right]\right\} \tag{76}$$

where $F[\mathbf{R}(\tau)]$ is known as the *influence functional*. From the form of $F[\mathbf{R}(\tau)]$, it is clear that this quantity is a partition function for the electronic subsystem along a given nuclear path $\mathbf{R}(\tau)$. At a fixed nuclear configuration, $\mathbf{R}$, this partition function could be computed from the electronic eigenvalues, $\varepsilon_n(\mathbf{R})$ and would be related to the negative exponential of the free energy:

$$F(\mathbf{R}) = \sum_n e^{-\beta\varepsilon_n(\mathbf{R})} = e^{-\beta A(\mathbf{R})} \tag{77}$$

where $A(\mathbf{R})$ is the free energy at nuclear configuration, $\mathbf{R}$. In the Born-Oppenheimer approximation, adiabaticity must be assumed along a nuclear path, i.e. at each τ, the electronic eigenvalue problem is solved for the specific configuration, $\mathbf{R}(\tau)$, at this imaginary time point. This means that the influence functional, $F[\mathbf{R}(\tau)]$, and hence the free energy, must be local in τ. This leads to a convenient expression for the path integral:

$$Z(N,V,T) = \oint \mathcal{D}\mathbf{R}(\tau)\ \exp\left\{-\frac{1}{\hbar}\int_0^{\beta\hbar}\left[T_{\mathrm{N}}(\dot{\mathbf{R}}(\tau)) + V_{\mathrm{NN}}(\mathbf{R}(\tau)) + A(\mathbf{R}(\tau))\right]\right\} \tag{78}$$

known as the free energy Born-Oppenheimer path integral approximation introduced by Cao and Berne[31].

On the other hand, if we simply consider the nuclear eigenvalue problem in Eq. (8), we would lead to a path integral expression in which we perform a separate path integral on each electronic surface, $\varepsilon_n(\mathbf{R})$ and then sum over the surfaces, i.e.

$$Z(N,V,T) = \sum_n \oint \mathcal{D}\mathbf{R}(\tau)\ \exp\left\{-\frac{1}{\hbar}\int_0^{\beta\hbar}\left[T_{\mathrm{N}}(\dot{\mathbf{R}}(\tau)) + V_{\mathrm{NN}}(\mathbf{R}(\tau)) + \varepsilon_n(\mathbf{R}(\tau))\right]\right\} \tag{79}$$

Differences between these two path integral expressions are discussed in detail by Cao and Berne[31]. It is important to note that when only the electronic ground state is important, the two expressions are equivalent, since, then

$$F[\mathbf{R}(\tau)] = \exp\left[-\frac{1}{\hbar}\int_0^{\beta\hbar} d\tau\ \varepsilon_0(\mathbf{R}(\tau))\right] \tag{80}$$

and the path integral expression reduces to

$$Z(N,V,T) = \oint \mathcal{D}\mathbf{R}(\tau)\ \exp\left\{-\frac{1}{\hbar}\int_0^{\beta\hbar}\left[T_{\rm N}(\dot{\mathbf{R}}(\tau)) + V_{\rm NN}(\mathbf{R}(\tau)) + \varepsilon_0(\mathbf{R}(\tau))\right]\right\} \tag{81}$$

which is the form on which we shall focus here.

The Born-Oppenheimer path integral form in Eq. (81) can be written as a discrete path integral:

$$\begin{aligned} Z_P(N,V,T) = &\left[\prod_{I=1}^{N}\left(\frac{M_I P}{2\pi\beta\hbar^2}\right)^{3P/2}\int d\mathbf{R}_I^{(1)}\cdots d\mathbf{R}_I^{(P)}\right] \\ &\times\exp\left\{-\beta\left[\sum_{i=1}^{P}\left(\sum_{I=1}^{N}\frac{1}{2}M_I\omega_P^2\left(\mathbf{R}_I^{(i+1)}-\mathbf{R}_I^{(i)}\right)^2\right.\right.\right. \\ &\left.\left.\left.+\frac{1}{P}\varepsilon_0(\mathbf{R}_1^{(i)},...,\mathbf{R}_N^{(i)})\right)\right]\right\} \end{aligned} \tag{82}$$

where the true partition function $Z(N,V,T) = \lim_{P\to\infty} Z_P(N,V,T)$ by virtue of the Trotter Theorem. We have already seen that discrete path integrals of this type can be evaluated by molecular dynamics (MD) using the staging or normal mode transformations and a Nosé-Hoover chain thermostat on each degree of freedom. However, there is a key point: the ground state electronic eigenvalue, $\varepsilon_0(\mathbf{R})$ must be evaluated at each imaginary time slice, $i = 1, ..., P$, i.e. at P different nuclear configurations. As dictated by the Born-Oppenheimer approximation, this requires P *separate electronic structure calculations*, thus, P sets of Kohn-Sham orbitals! This is somewhat unfortunate, as electronic structure calculations are already expensive enough for a single nuclear configuration. Now, each path discrete configuration requires P electronic structure calculations! The one saving grace is that the P electronic structure calculations are entirely independent of each other and can, therefore, be performed in parallel with no communication overhead. Thus, combining the staging or normal mode path integral method with the Car-Parrinello equations of motion for each set of Kohn-Sham orbitals, one arrives at the complete set of *ab initio* path integral equations of motion:

$$\begin{aligned} \mu|\ddot{\psi}_i^{(s)}\rangle &= |\tilde{\varphi}_i^{(s)}\rangle + \sum_\alpha \lambda_\alpha^{(s)} - \sum_j \Lambda_{ij}|\psi_i^{(s)}\rangle - \mu\dot{\eta}_1^{(s)}|\dot{\psi}_i^{(s)}\rangle \\ M_I^{'(s)}\ddot{u}_I^{(s)} &= -M_I^{(s)}\omega_P^2 u_I^{(s)} - \frac{1}{P}\frac{\partial\tilde{E}^{(s)}}{\partial u_I^{(s)}} - M_I^{'(s)}\dot{\xi}_{1_I}^{(s)}\dot{u}_I^{(s)} \\ Q_R\ddot{\xi}_{I,\nu}^{(s)} &= \tilde{G}_{I,\nu}^{(s)} - Q_R\dot{\xi}_{I,\nu}^{(s)}\dot{\xi}_{I,\nu+1}^{(s)} \qquad \nu = 1,...,M-1 \\ Q_R\ddot{\xi}_{I,M}^{(s)} &= \tilde{G}_{I,M}^{(s)} \\ Q_\kappa\ddot{\eta}_\kappa^{(s)} &= \gamma_\kappa^{(s)} - Q_\kappa\dot{\eta}_\kappa^{(s)}\dot{\eta}_{\kappa+1}^{(s)} \qquad \kappa = 1,...,M-1 \\ Q_M\ddot{\eta}_M^{(s)} &= \gamma_M^{(s)} - Q_M\dot{\eta}_{M-1}^{(s)}\dot{\eta}_M^{(s)} \end{aligned} \tag{83}$$

where s indexes the imaginary time slices, and $Q_R = 1/(\beta\omega_P^2)$. The ionic thermostat forces are given by

$$\tilde{G}_{I,1}^{(s)} = \tilde{M}_I(\dot{u}_I^{(s)})^2 - kT$$

$$\tilde{G}_{I,\nu}^{(s)} = Q_R(\dot{\xi}_{I,M-2}^{(s)})^2 - kT \tag{84}$$

The electronic thermostat forces are given by

$$\begin{aligned}
\gamma_1^{(s)} &= \mu \sum_i \langle \dot{\psi}_i^{(s)} | \dot{\psi}_i^{(s)} \rangle - E_e \\
\gamma_{M-1}^{(s)} &= \left[Q_{M-2} \left(\dot{\eta}_{M-2}^{(s)} \right)^2 - \frac{1}{\beta_e} \right] + \left[Q_M \left(\dot{\eta}_M^{(s)} \right)^2 - \frac{1}{\beta_e} \right] \\
\gamma_\kappa^{(s)} &= Q_{\kappa-1} \left(\dot{\eta}_{\kappa-1}^{(s)} \right)^2 - \frac{1}{\beta_e} \qquad \kappa = 2, ..., M-2, M
\end{aligned} \tag{85}$$

E_e is the desired electronic kinetic energy, and $1/\beta_e = E_e/N_e$, where N_e is the number of fictitious dynamical degrees of freedom. The thermostat masses are given by $Q_1 = 2E_e/\omega_e^2$, $Q_\kappa = 1/(\beta_e\omega_e^2)$, $\kappa = 2, ..., M$. ω_e is a characteristic frequency for the fictitious electron dynamics and is usually taken to be several times larger than the highest frequency of the nuclear motion. In practice, one might choose N_e to be somewhat smaller than the actual number of electronic degrees of freedom in order to avoid a large thermostat mass disparity[32]. Eqs(83) are sufficiently general to allow inclusion of ultrasoft pseudopotentials in a straightforward manner, however, they are not limited to this choice.

5 Illustrative Applications

5.1 Structure of Liquid Ammonia at 273 K

Ammonia is an important weakly hydrogen-bonded liquid that is employed as a solvent in many common organic reactions and in solutions with metals. Its structure has recently been determined experimentally by neutron diffraction[33] so that experimental partial structure factors and radial distribution functions are now available. As a study of chemical processes in ammonia solvent is a prime application for AIMD techniques, it is important to validate the approach by studying the properties of the neat liquid and making a detailed comparison with experiment.

To this end, AIMD simulations based on the CP equations of motion have been carried out on a sample of 32 ammonia molecules in a box of length 11.27 Åwith periodic boundary conditions[12,13]. Exchange and correlation were treated using the B-LYP GGA functional[34,35] and the KS orbitals were expanded in a plane wave basis up to a cutoff of 70 Ry. Core electrons were treated using the pseudopotentials of Troullier and Martins[24]. The system was allowed to equilibrate for 2.2 ps and then a production run of 6.0 ps was carried out using a time step of 5 a.u.

Figure 1 shows the computed neutron scattering partial structure factors, $H_{\rm NN}(q)$, $H_{\rm HH}(q)$, and $H_{\rm NH}(q)$ together with the experimental results. As can bee seen, very good

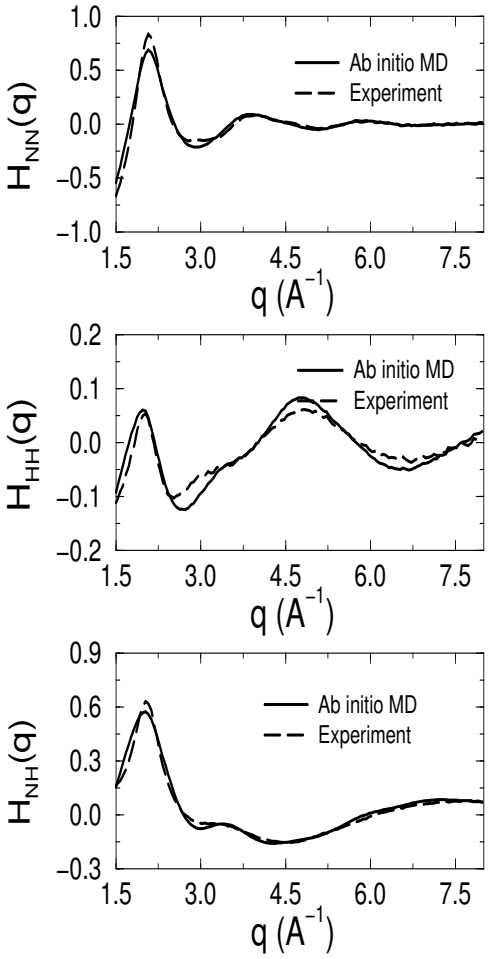

Figure 1. Computed and experimental neutron scattering partial structure factors for liquid ammonia at 273 K

agreement with experiment is obtained. In addition, we show the computed and experimentally determined radial distribution functions in Fig. 2. In addition, the self diffusion constant was determined from the calculation to be 1.1×10^{-4} cm^2/s, which compares favorably with the experimental value of $1.0\times10-4$ cm^2/s.

5.2 Structure of Liquid Methanol at 300 K

Another important hydrogen-bonded liquid is methanol (CH_3OH). Like ammonia, methanol is also used as a solvent in many common organic reactions. It is also a industrially important liquid because of its role in emerging fuel-cell technologies. The structure of liquid methanol has also been determined recently by neutron diffraction[36,37], again, making partial structure factors and radial distribution functions readily available for com-

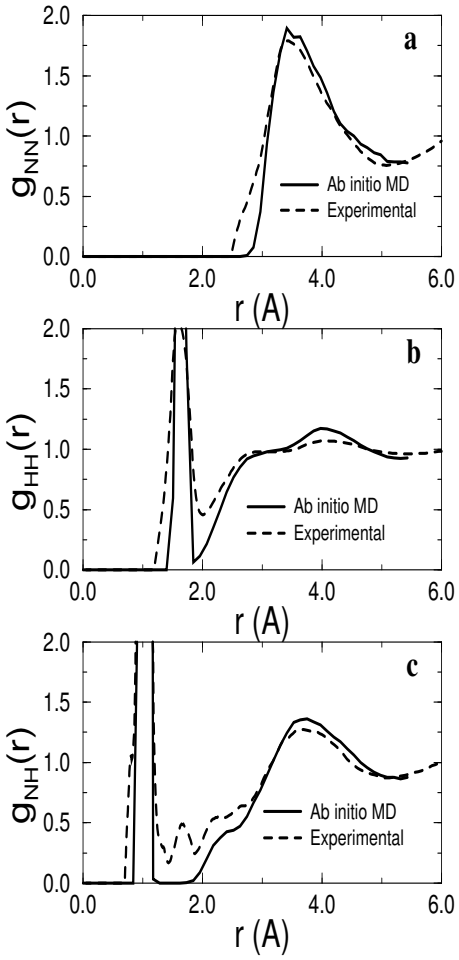

Figure 2. Computed and experimental radial distribution functions for liquid ammonia at 273 K

parison with AIMD calculations. We have recently carried out studies of proton transport in liquid methanol and methanol/water mixtures[17], and as part of these studies, we carried out a simulation of the pure liquid in order to compare the structural properties with those determined experimentally.

The AIMD simulation protocol employed 32 methanol molecules in a periodic box of 12.93 Å. Exchange and correlation were, again, treated using the B-LYP GGA functional, and, because of the large system size (the system consists of 192 atoms and 224 electronic states), core electrons were treated using the ultrasoft pseudopotential approach of Vanderbilt[25]. This allowed the plane wave basis set expansion to be truncated at a cutoff of 25 Ry. The system was equilibrated for 4 ps, and a production run of 20 ps was then carried out using a time step of 5 a.u.

Figure 3 shows the computed and experimentally determined partial structure factors. The heavy-atom partial structure factor is a linear combination of individual partial struc-

ture factors:

$$H_{\mathrm{XX}}(q) = 0.042H_{\mathrm{CC}}(q) + 0.073H_{\mathrm{CO}}(q) + 0.253H_{\mathrm{CM}}(q) + 0.032H_{\mathrm{OO}}(q) \qquad (86)$$

where M denotes a methyl hydrogen. Again, it can be seen that good agreement is

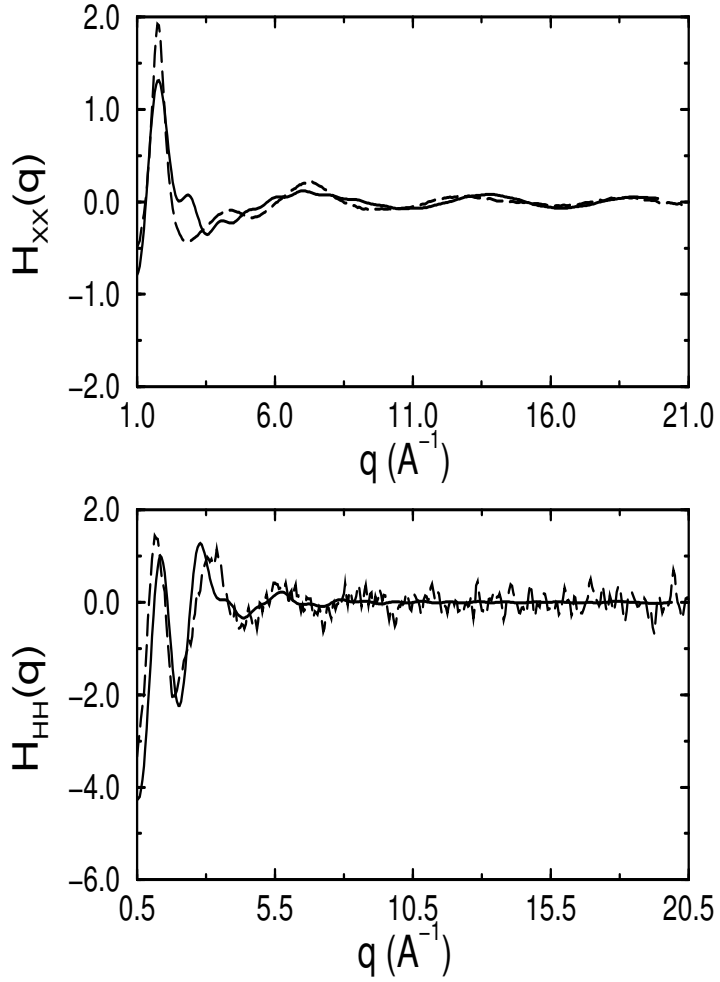

Figure 3. Computed (solid line) and experimental (dashed line) neutron scattering partial structure factors for liquid methanol at 300 K

obtained, although, for this system, the experimental data is somewhat noisier. Figure 4 shows the 10 different radial distribution functions plotted against the experimentally determined radial distribution functions. In all cases, good agreement is obtained. This

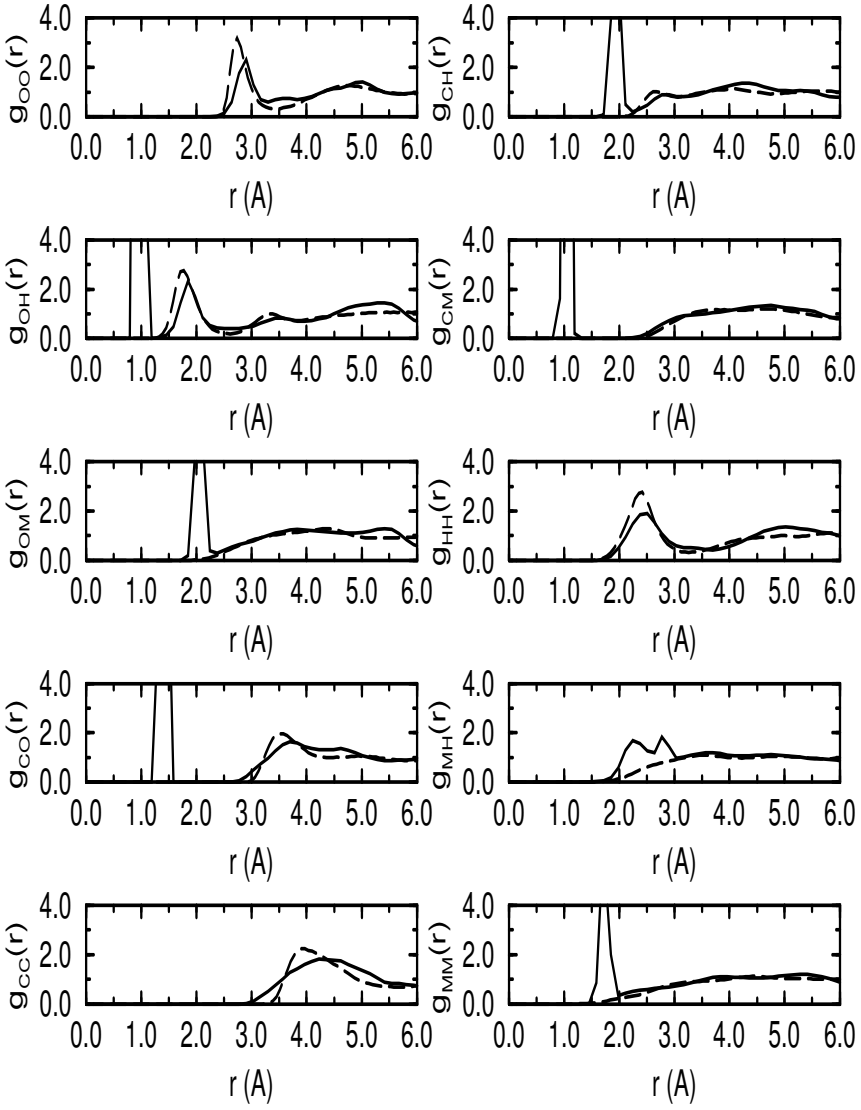

Figure 4. Computed (solid line) and experimental (dashed line) radial distribution functions for liquid methanol at 300 K

and the previous study, as well as numerous studies of liquid water[2–7] show that the AIMD method is capable of treating a variety of hydrogen-bonded systems accurately.

5.3 Proton Transfer in Malonaldehyde

One of the main advantages of the AIMD technique is that it allows the study of chemical bond-breaking and forming events, for which reliable empirical potential models generally do not exist. As an illustration of the AIMD and AIPI methods, we investigate the role of

nuclear quantum effects on a very common chemical reaction, the proton transfer reaction. Here, a simple example, proton transfer through the internal hydrogen bond in the malonaldehyde molecule is explored[38]. The process is illustrated in Fig. 5 below. As the figure

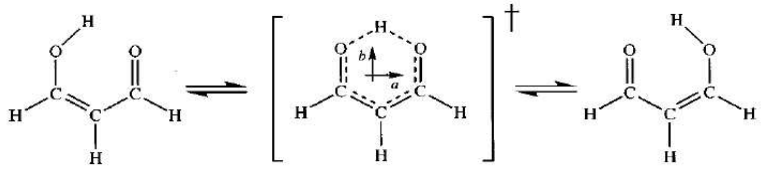

Figure 5. Illustration of the proton transfer process in malonaldehyde

makes clear, the transfer of the proton between the two oxygens gives rise to a change in the chemical bonding pattern around the ring. At zero temperature, the barrier to proton transfer, as computed by high level *ab initio* calculations ranges from 3.1 kcal/mol to 4.6 kcal/mol.

Our AIMD and AIPI simulations are based on the use of the Becke GGA exchange[34] and Perdew-Zunger[40] correlation functionals. The malonaldehyde molecule was placed in an 8.0 Åperiodic box, and a plane-wave cutoff of 70 Ry was employed. Core electrons were treated using the Troullier-Martins pseudopotentials[24]. This DFT scheme gives a zero-temperature proton transfer barrier of 3.5 kcal/mol, in good agreement with the aforementioned estimates. In addition, for path integral calculations, a discretization of $P = 16$ imaginary time slices was employed. In this study, three different types of calculations were performed: 1) all nuclei treated as classical point particles; 2) all nuclei treated as quantum particles; 3) quantization of *only* the transferring proton (called *classical skeleton* calculations). In each case, thermodynamic integration in conjunction with the bluemoon ensemble approach[39] is used to obtain the proton transfer fre energy profile at 300 K.

Figure 6 shows the free energy profiles thus obtained for each of the three simulation types. The reaction coordinate on the x-axis is $\nu = d_{\mathrm{O_1H}} - d_{\mathrm{O_2H}}$, the difference between the distances of each oxygen to the shared proton. The most striking features of these profiles are i) that inclusion of only thermal fluctuations, via the classical nuclei simulation, gives rise to very little difference between the free energy and zero-temperature barriers. When the transferring proton only is quantized, the barrier is considerably lower (approximately 2.1 kcal/mol). Finally, when all nuclei are properly quantized, the barrier is further lowered to approximately 1.6 kcal/mol. This implies that there is a nontrivial quantum effect due to the heavy-atom skeleton. Failure to include this quantum effect leads to an overestimation of the free energy barrier of 31%. (and, hence, underestimation of the proton transfer rate by a factor of roughly 2 in a transition state theory picture[41]). We note that our classical skeleton approximation is a comparatively mild one in comparison to approximations that are commonly made in the modeling of such processes. The latter usually completely disregard the structure of the heavy-atom skeleton or attempt to reduce the dimensionality of the problem to a few relevant degrees of freedom. Therefore, the classical skeleton approximation most likely leads to a lower bound estimate of the amount by which more severe approximations would tend to overestimate the free energy

barrier and underestimate the rate.

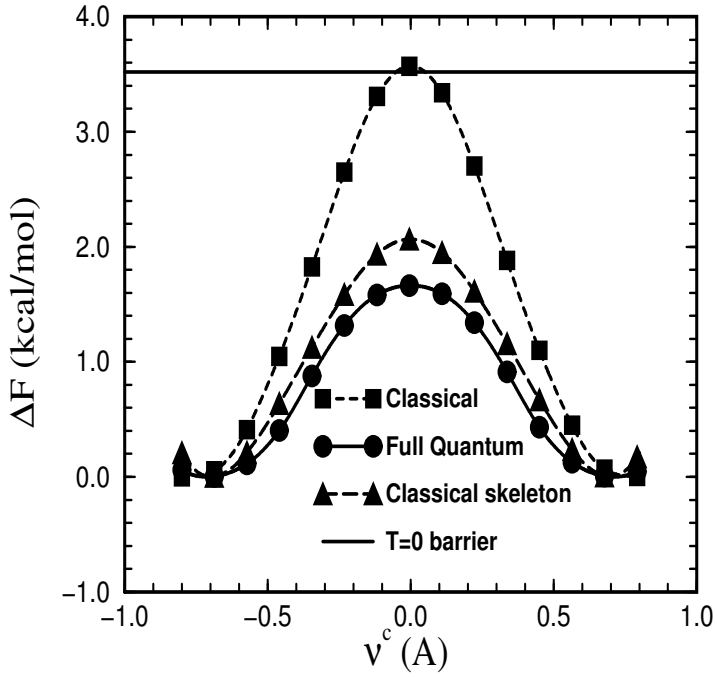

Figure 6. Proton transfer free energy profiles in malonaldehyde

5.4 Proton Transport in Water

Aqueous proton transport is a fundamentally important process in the chemistry of acids and bases and in many biologically important systems. In water, protonic defects (hydronium, H_3O^+, and hydroxide, OH^-, ions) have an anomalously high mobility that cannot be explained by an ordinary hydrodynamic diffusion picture. In fact, the commonly accepted mobility mechanism is the so called "structural diffusion" or "Grotthuss" mechanism, in which solvation structures diffuse through the hydrogen-bond network via sequential proton transfer reactions. However, the microscopic details of the Grotthuss mechanism for different situations remain largely unelucidated. Here, we describe AIMD and AIPI simulations[4–7] that have lead to a clear picture of the structural diffusion mechanism of the hydronium ion in water, a picture that has since been shown to be consistent with all available experimental data[42]. In addition, one of the key controversial issues, concerning the dominant solvation structures, is resolved. Briefly, one school of thought, put forth by Eigen, considers the dominant solvation structure to be that of a H_3O^+ core surrounded

by three water molecules consisting of a $H9O_4^+$ cation. The other shool of thought, due to Zundel, favors a picture in which the dominant structure consists of a protonated water dimer or $H_5O_2^+$ cation, in which the proton is equally shared between two water molecules.

The simulation protocol consists of 31 water molecules and one hydronium ion in a 10 Åperiodic box. Exchange and correlation are, again, treated using the B-LYP functional, and a plane wave basis set truncated at a cutoff of 70 Ry was employed. Core electrons were treated using the Troullier-Martins pseudopotentials. For path integral simulations, a discretization of 8 imaginary time slices was employed. AIMD and AIPI trajectories of length 20 ps using a time step of 7 a.u. were generated.

Figure 7 shows schematically the structural diffusion mechanism that is uncovered in these simulations. As the figure shows, the process involves the breaking of a hydrogen

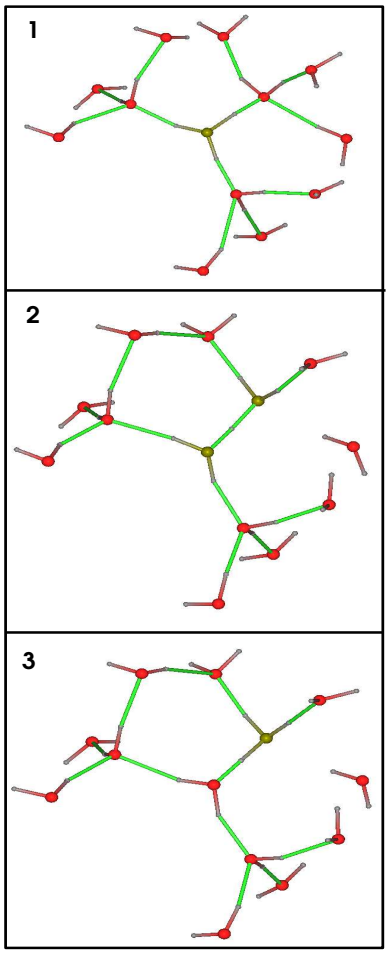

Figure 7. Schematic of the hydronium transport mechanism in water. The figure shows the hydronium and its first two solvation shells.

bond between the first and second solvation shell members of H_3O^+, i.e., a second solvation shell fluctuation[4,5]. Following this hydrogen-bond breaking event, a first solvation shell water is left in a state in which its coordination is 3 instead of the usual average value of 4 for water. In this state, it is coordinated more like hydronium than water, and it is, therefore, "prepared" to become a properly solvated hydronium via proton transfer. When its coordination number changes, the oxygen-oxygen distance between the hydronium and the undercoordinated water shrinks by approximately 0.1 Å, and the proton moves to the middle of the bond, forming an intermediate $H_5O_2^+$ cation state. The proton can then either return to the original hydronium or continue to cross the hydrogen bond to the new oxygen site. If the latter occurs, then there is a new $H_9O_4^+$ cation formed with a new hydronium core. Thus, the solvation structure has migrated through the hydrogen bond network via the proton transfer step. The rate-limiting process is the hydrogen bond-breaking event, which requires approximately 1.5 ps to occur. This number is in good agreement with the experimentally determined rate of structural diffusion from NMR measurements[43]. In addition, the activation enthalpy, approximately 3 kcal/mol, can be explained by this mechanism, which requires approximately 2.5 kcal/mol to break the hydrogen bond and another 0.5 kcal/mol to shrink the oxygen-oxygen distance after the hydrogen bond is broken[44].

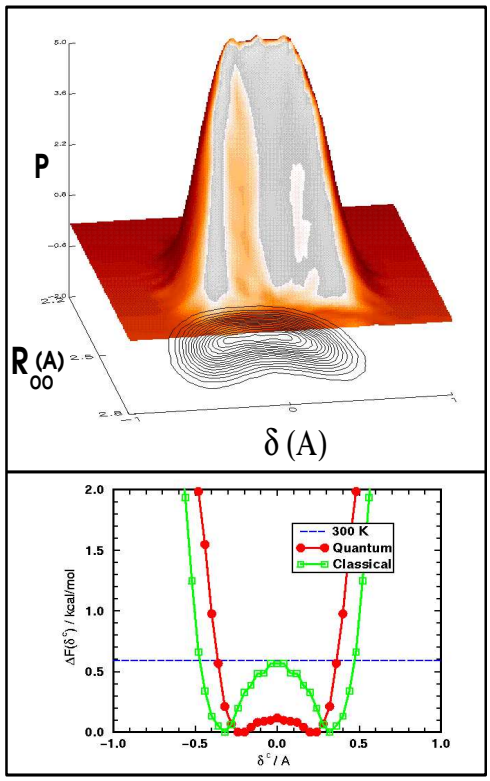

Figure 8. Quantum probability distribution of the proton transfer reaction coordinate, δ and the oxygen-oxygen distance, R_{OO}.

Inclusion of nuclear quantum effects via the path integral can resolve the controversy of the solvation structures[6,7]. In particular, if we plot the probability distribution of the oxygen-oxygen distance, $R_{\rm OO}$ and the proton transfer coordinate, δ (similar to the coordinate, ν, described above) for the hydrogen bond in which proton transfer is "most likely to occur" (defined as the hydrogen bond with the smallest value of δ), which is shown in Fig. 8, we see that the probability that the solvation complex is $H_9O_4^+$ or $H_5O_2^+$ or any complex in between these two ideal, limiting structures is approximately the same. This is also confirmed by studying the free energy profile along the coordinate, δ also shown in Fig. 8. The fact that there is a broad flat minimum in this free energy confirms the notion that there is no single dominant solvation structure. Rather, the defect is best described as a "fluxional" defect, that can take on, with same probability, the characteristics of the $H_9O_4^+$ or $H_5O_2^+$ cations and all structures in between these. Interestingly, a purely classical treatment of the predicts that the $H_9O_4^+$ is considerably more stable than the $H_5O_2^+$ cation by approximately 0.6 kcal/mol. This proton transfer barrier is completely washed out by nuclear zero-point motion, leading to the fluxional defect picture proposed in Ref.[7].

References

1. R. Car and M. Parrinello, *Phys. Rev.Lett.* **55**, 2471 (1985).
2. P. L. Silvestrelli and M. Parrinello, *J. Chem. Phys.* **111**, 3572 (1999).
3. P. L. Silvestrelli, M. Bernasconi and M. Parrinello, *Chem. Phys. Lett.* **277**, 478 (1997).
4. M. E. Tuckerman, K. Laasonen, M. Sprik and M. Parrinello, *J. Chem. Phys.* **103**, 150 (1995).
5. M. E. Tuckerman, K. Laasonen, M. Sprik and M. Parrinello, *J. Phys. Chem.* **99**, 5749 (1995).
6. D. Marx, M. E. Tuckerman, J. Hutter, and M. Parrinello, *Nature* **397**, 601 (1999).
7. D. Marx, M. E. Tuckerman and M. Parrinello, *J. Phys. Condens. Matt.* **12**, A153 (2000).
8. M. Bernasconi, P. L. Silvestrelli and M. Parrinello, *Phys. Rev. Lett.* **81**, 1235 (1998).
9. M. Benoit, D. Marx and M. Parrinello, *Nature* **392**, 258 (1998).
10. J. Sarnthein, A. Pasquarello and R. Car, *Science* **275**, 1925 (1997).
11. M. Benoit, S. Ispas and M. E. Tuckerman, *Phys. Rev. B* **64**, 224205 (2991).
12. M. Diraison, G. J. Martyna and M. E. Tuckerman, *J. Chem. Phys.* **111**, 1096 (1999).
13. Y. Liu and M. E. Tuckerman, *J. Phys. Chem. B* **105**, 6598 (2001).
14. S. Piana, D. Sebastiani, P. Carloni and M. Parrinello, *J. Am. Chem. Soc.* **123**, 8730 (2001).
15. J. Hutter, P. Carloni and M. Parrinello, *J. Am. Chem. Soc.* **118**, 871 (1996).
16. M. Boero and M. Parrinello, *J. Am. Chem. Soc.* **122**, 501 (2000).
17. J. A. Morrone and M. E. Tuckerman (to be submitted).
18. Z. H. Liu, L. E. Carter and E. A. Carter, *J. Phys. Chem.* **99**, 4355 (1995).
19. B. Di Martino, M. Celino and V. Rosato, *Comp. Phys. Comm.* **120**, 255 (1999).
20. R. A. Friesner, *Chem. Phys. Lett.* **116**, 39 (1985).
21. G. Lippert, J. Hutter and M. Parrinello, *Mol. Phys.* **92**, 477 (1997).
22. Y. Liu and M. E. Tuckerman (to be submitted).
23. G. B. Bachelet, D. R. Hamann, and M. Schlüter, *Phys. Rev. B.* **26**, 4199 (1982).

24. N. Troullier and J. Martins, *Phys. Rev. B* **43**, 6796 (1991).
25. D. Vanderbilt, *Phys. Rev. B* **41**, 7892 (1990).
26. P. E. Blöchl, *Phys. Rev. B* **50**, 17953 (1994).
27. L. Kleinman and D. M. Bylander, *Phys. Rev. Lett.* **48**, 1425 (1982).
28. G. J. Martyna and M. E. Tuckerman, *J. Chem. Phys.* **110**, 2810 (1999).
29. P. Minary, M. E. Tuckerman, K. A. Pihakari and G. J. Martyna, *J. Chem. Phys.* (in press).
30. R. P. Feynman and F. L. Vernon, *Ann. Phys.* **24**, 118 (1963).
31. J. Cao and B. J. Berne, *J. Chem. Phys.* **99**, 2902 (1993).
32. M. E. Tuckerman and M. Parrinello, *J. Chem. Phys.* **101**, 1302 (1994).
33. M. A. Ricci, N. Nardone, F. P. Ricci, C. Andreani and A. K. Soper, *J. Chem. Phys.* **102**, 7650 (1995).
34. A. D. Becke, *Phys. Rev. A* **38**, 3098 (1988).
35. C. Lee, W. Yang, and R. C. Parr, *Phys. Rev. B* **37**, 785 (1988).
36. T. Yamaguchi, K. Hidaka and A. K. Soper, *Mol. Phys.* **96**, 1159 (1999).
37. S. Dixit, W. C. K. Poon, and J. Crain, *J. Phys. Condens. Matt.* **12**, L323 (2000).
38. M. E. Tuckerman and D. Marx, *Phys. Rev. Lett.* **86**, 4946 (2001).
39. M. Sprik and G. Ciccotti, *J. Chem. Phys.* **109**, 7737 (1998).
40. J. Perdew and A. Zunger, *Phys. Rev. B* **23**, 5048 (1981).
41. G. A. Voth, *J. Phys. Chem.* **97**, 8365 (1993).
42. N. Agmon, *Chem. Phys. Lett.* **244**, 456 (1995).
43. S. Meiboom, *J. Chem. Phys.* **34**, 375 (1961).
44. N. Agmon, *J. Molec. Liq.* **73,74**, 513 (1997).